Applied Catalysis B: Environmental 84 (2008) 607–615

Contents lists available at ScienceDirect

Applied Catalysis B: Environmental

journal homepage: www.elsevier.com/locate/apcatb

Preparation, active phase composition and Pd content of perovskite-type oxides

E. Tzimpilis [a,*], N. Moschoudis [a], M. Stoukides [a,b], P. Bekiaroglou [a]

[a] Department of Chemical Engineering, Aristotle University of Thessaloniki, 54124 Thessaloniki, Greece
[b] Chemical Process Engineering Research Institute, University Box 1517, 54124 Thessaloniki, Greece

ARTICLE INFO

Article history:
Received 19 March 2008
Received in revised form 13 May 2008
Accepted 17 May 2008
Available online 28 May 2008

Keywords:
Pd catalyst
Pd-perovskites
Natural gas vehicles

ABSTRACT

Perovskite-type oxides, containing Pd, were prepared via a combined sol–gel and combustion synthesis method and were characterized by X-ray diffraction (XRD), transmission electron microscopy (TEM), X-ray photoelectron spectroscopy (XPS) and BET specific surface area (SSA). Their activity as three-way catalysts for the abatement of carbon monoxide, methane and nitrogen oxides, emitted from stoichiometrically operating natural-gas-fuelled vehicles, was investigated under simulated exhaust conditions. The preparation conditions concerning the complexing agent, the use of additives and the thermal treatment of the precursor solutions, were investigated. The $La_{0.91}Mn_{0.85}Ce_{0.24}Pd_{0.05}O_z$ and $La_{1.034}Mn_{0.966}Pd_{0.05}O_z$ phases were the most active. Their activation by high-temperature hydrothermal treatment was ascribed to the migration of Pd out of the perovskite lattice and the formation of segregated PdO. The role of Pd was crucial for the catalytic activity of the active phase. A low Pd content favored the dispersion of oxidized Pd^{x+}, $2 \leq x \leq 4$, and thus, enhanced catalytic activity. Oxidized Pd^{x+} with $x > 2$ appeared to be less active than Pd^{2+}. The catalytic activity of $La_{1.034}Mn_{0.966}Pd_{0.05}O_z$ increased significantly when 8 ppm SO_2 were introduced in the reaction mixture.

1. Introduction

Methane is the main component of natural gas, an abundant raw material. An important application of natural gas is its use as a fuel for vehicles. Compared to gasoline, it exhibits reduced emissions during cold start and low particulate matter, while its low carbon to hydrogen ratio implies lower CO_2 emissions and less contribution to the greenhouse effect. Nevertheless, CO and unburned methane, which is a powerful greenhouse gas, are present in the exhaust stream. Moreover, in the natural gas fuelled vehicles (NGFVs) operating under stoichiometric fuel to air conditions, NO_x emissions are present too, in contrast to the lean-burn NGFVs in which the low operation temperature, $<550\,^{\circ}C$, does not favor NO_x formation [1,2]. Consequently, three-way exhaust aftertreatment is necessary for the abatement of CH_4, CO and NO_x emissions from stoichiometrically operating NGFVs.

Palladium, in its oxidized form (PdO), is the most active catalyst for methane oxidation and has been extensively studied in the past [3–6]. The use of perovskite-type oxides represented by the general formula ABO_3, as catalysts for complete oxidation of HCs is widely being investigated since the 1970s in order to (a) decrease the cost and (b) enhance the thermal stability towards high-temperature sintering [7–9]. Noble metal-containing perovskites have been tested as catalysts for CO oxidation, oxidation of methane to syngas, oxidation of volatile organic compounds and the CO + NO reaction [10–14]. Doped perovskites with noble metals have also been investigated as catalysts for the catalytic flameless combustion (CFC) of methane [15–18] and as potential substitutes of the current three-way catalysts (TWCs) for gasoline [19–22] and NGFVs [23].

A number of parameters such as the active phase composition, the preparation procedure, the feed stream composition, the thermal treatment and the operating conditions, appear to affect the performance of perovskites as TWCs for NGFVs. The preparation method is of crucial importance for the properties of the obtained materials [24]. Campagnoli et al. [9] found that $LaMnO_3$ perovskites prepared by different preparation methods exhibited different BET specific surface areas (SSA), crystallization extent, catalytic activity and thermal stability for the CFC of methane. Natile et al. [25] reported similar observations for $LaCoO_3$ and Giannakas et al. [26] for $LaMO_3$ (M = Mn, Fe). Oliva et al., found that minute changes in the preparation procedure can have a remarkable effect on the physico-chemical characteristics and the catalytic properties of perovskites [27]. In addition to the preparation process, introduction of 10 vol% water vapor in the feed stream was found to decrease the catalytic activity of $LaBO_3$ (B: Co, Mn, Fe) [22]. This was attributed to a competition between

* Corresponding author. Tel.: +30 2310996178; fax: +30 2310996222.
E-mail address: tzimpi@auth.gr (E. Tzimpilis).

0926-3373/$ – see front matter © 2008 Elsevier B.V. All rights reserved.
doi:10.1016/j.apcatb.2008.05.016

water and reactants (NO, C_3H_6, O_2) for the active sites. It was also found that insertion of Pd in $LaFeO_3$ improved the water resistance [22]. The same explanation was proposed for the deactivation by water steam in the feed of Pd/Al_2O_3 and Pt/Al_2O_3 TWCs of a lean-burn NGFV [28]. Perovskite catalysts are also sensitive to sulfur poisoning, since only a few ppm of SO_2 can cause deactivation [29,30]. In the case of Pd/Al_2O_3 for lean-burn NGFVs, it was found that 1 ppm SO_x in the exhaust, inhibits remarkably the oxidation of methane [3]. Substitution of A and/or B cations in the perovskite structure was found to improve the SO_2 resistance. Moreover, promising results regarding SO_2, were obtained by addition to or incorporation of noble metals in the perovskite structure [31].

Because of the stability of the methane molecule, the catalytic converter of NGFVs must fulfill certain requirements: high catalytic activity, thermal stability, SO_2 resistance and selectivity to NO_x reduction. Most of the studies of catalytic exhaust aftertreatment of NGFVs refer to lean-burn operation with noble metals supported on alumina. Only a few papers for operation at, or close to stoichiometry, can be found [5,32].

In the present study the effects of (a) active phase composition, (b) preparation, (c) thermal treatment and (d) sulfur attack, on the capability of Pd containing perovskites for use as TWCs of stoichiometrically operating NGFVs, are investigated. The active phases used are based on $LaMnO_3$ and have the general formula $La_kMn_mA_nPd_xO_z$ (A = Ce, Mg, Zr, $k + m + n = 2$, $n = 0.00, 0.24$). The goal of this work is to optimize the performance of TWCs via minimization of their Pd content.

2. Experimental

2.1. Catalysts preparation

A combined sol–gel and combustion synthesis method was applied for the preparation of the perovskite-type oxides. This combination is based on the dual role of glycine in the preparation procedure: (a) as the complexing agent to ensure the homogeneity of the gel that is formed during evaporation and (b) as the internal fuel, which reacts with the internal oxidants (nitrogen oxides formed during the decomposition of the nitrates) and/or atmospheric oxygen at about 300 °C. The preparation conditions were varied in order to examine their effect on the catalytic activity of the obtained powders. The precursor solutions were prepared using appropriate quantities of 2 M aqueous solutions of the corresponding metal nitrates $La(NO_3)_3{\cdot}6H_2O$ (Merck), $Mn(NO_3)_2{\cdot}4H_2O$ (Merck), $Ce(NO_3)_2{\cdot}6H_2O$ (Merck), $Pd(NO_3)_2{\cdot}2H_2O$ $2H_2O$ (Fluka), $Mg(NO_3)_2{\cdot}6H_2O$ (Merck) and $ZrO(NO_3)_2{\cdot}xH_2O$ (Aldrich). Metal ions complexation was achieved by the addition of glycine (Merck) or urea (Fluka) in suitable excess. NH_4NO_3 (Fluka) was used as additive, in order to achieve high-temperature rise in the bulk of the prepared powders during calcination. The resulted homogenous precursor solutions were either undergone evaporation at 115 °C for 24 h, forming an amorphous material that was crashed and calcined in air at 500 °C (dry-500) or 750 °C (dry-750), or were directly introduced in the furnace for calcination (liquid-500 or liquid-750). The powders obtained were catalytically tested in two forms. In the first, 0.9–1.1 mm sized granules were introduced in the reactor for fast screening and optimization of the preparation procedure and the active phase composition. In the second, the powders were deposited on monolithic cordierite substrates of 400 cpsi (Corning) in order to approach real conditions. Deposition was achieved by immersing into slurries of active phase powders in *n*-butanol (J.T. Baker), followed by drying at 120 °C and calcination in air at 750 °C for 1 h. The resulted coated monoliths, 6 × 6 cells and 18 mm length, had negligible mass loss during experiments. Before the catalytic activity measurements, the catalysts underwent further thermal treatment in air or in reactant mixtures (compositions presented in Section 2.2) at 750 °C or 950 °C for several hours.

Table 1
Reactant mixture compositions (mol%) for activity tests and thermal treatments

Component	Composition 1	Composition 2	Composition 3
CH_4	0.10	0.05	0.05
CO	0.40	0.50	0.50
NO	–	0.10	–
O_2 (determined by R_x)	0.6000 (R_x = 1.5)	0.3700 (R_x = 1.2) 0.3070 (R_x = 1.02) 0.2965 (R_x = 0.99) 0.2860 (R_x = 0.96)	0.4200 (R_x = 1.2)
CO_2	10.00	10.00	10.00
H_2O	10.00	10.00	10.00
SO_2	0.0005 (optional)	0.0008 (optional)	–
N_2	Balance	Balance	Balance

2.2. Catalytic activity measurements

The catalytic activity tests and the high-temperature thermal treatment of the samples were carried out in a tubular quartz reactor. The external surface of the monolithic catalysts was covered by sufficient quantity of inactive ceramic wool, which was properly compressed, in order to avoid the passages of the gaseous reactants between the monolith external surface and the internal one of the quartz tube. A thermocouple at the front side of the catalytic bed or the monolith was used for the inlet temperature measurement. All catalysts were tested by applying the temperature programmed reaction technique in the temperature range 300–800 °C. The samples were either warmed up at a rate of 10 °C min^{-1} or free cooled down. To obtain high catalytic activity, each heating–cooling cycle started from 800 °C. The space velocity was 100 000, 100 000 or 50 000 and 50 000 h^{-1}, for the granulated, monolithic, and the thermal treatment, respectively.

The stoichiometric number, R_x, was used to describe the gas feed redox characteristics. It is defined as the ratio of the sum of the equivalents of oxidants (oxygen, nitrogen monoxide) to the sum of the equivalents of reductants (methane, carbon monoxide):

$$R_x = \frac{2[O_2] + [NO]}{4[CH_4] + [CO]}$$

All concentrations are expressed in mol%.

The gas feed compositions used for the thermal treatments and for the catalytic activity measurements are shown in Table 1. Composition 1 was employed for the thermal treatments and the activity tests on the granulated catalysts and for the determination of the active phase load on the monolithic catalysts. Composition 2 was used for the simulation of representative real conditions and composition 3 for the thermal treatments of the monolithic catalysts.

Analysis of the reactor gas outlet was carried out on a series of continuous analyzers, in particular, an FID PM-1 (Pierburg) for total hydrocarbons, an NDIR Uras 10 E (Hartmann & Braun) for CO and N_2O, a CLD (Grubb Parsons Chemitox) for NO_x and a paramagnetic OXYNOS-1 (LEYBOLD-HERAEUS) for O_2.

2.3. Characterization

A series of characterization techniques were applied on fresh and thermally treated catalysts. The reactant mixture with the composition 1 in Table 1 was used for the thermal treatments. BET SSA of the catalytic powders was measured by nitrogen adsorption

at 77 K. Crystal phases were identified by X-ray diffraction (XRD) using a Siefert 3003-TT diffractometer with Fe Kα radiation (λ = 1.9361 Å), in the 2θ range 20–110°. Transmission electron microscopy (TEM) observations were performed by JEOL 120UX and 2010 FX electron microscopes operating at 100 and 200 kV, respectively. X-ray photoelectron spectroscopy (XPS) was applied for the determination of the surface elements atomic concentration and surface ions valence state. An ultra high vacuum SPECKS LHS-10 system with Al Kα radiation (1486.6 eV) was used. Binding energy measurements of samples that exhibited electrostatic surface charging, were corrected with reference to the C 1s peak at 284.4 eV.

3. Results and discussion

3.1. Catalytic activity tests

3.1.1. Granulated catalysts

A preliminarily optimized active phase with the composition $La_{0.91}Mn_{0.85}Ce_{0.24}Pd_xO_z$ ($x = 0.1$) was used as starting material for the determination of the optimum preparation procedure.

Fig. 1 shows the effect of complexing agent, use of additive and thermal treatment of the precursor solution, on the methane light off temperature, T_{50}, which corresponds to 50% conversion of methane. Before testing, all catalysts had undergone an ageing procedure at 950 °C for 5 h. The catalytic activity tests were done both, in the presence and in the absence of CO. The use of glycine as complexing agent and drying at 115 °C for 24 h before calcination at 750 °C resulted in the most active catalyst. A considerable increase in T_{50} was observed when the drying step was skipped or when a lower calcination temperature was applied. The use of urea gave promising results and, moreover, its preparation via the solution combustion synthesis was less time and energy consuming. Nevertheless, a comparison of glycine dry-750 and urea liquid-750 in the range 300–750 °C, showed that in the case of 0.4% CO, the former was superior below 450 °C and above 590 °C. The same was observed for CO free reacting mixtures at temperatures lower than 480 °C and higher than 670 °C. It is also interesting that all catalysts appeared more effective when CO was introduced in the reactant mixture. The stability of PdO in the Pd/γ-Al_2O_3 catalyst is reported to depend strongly on the reactant composition, especially on the nature of the reducer [33]. According to Cimino et al. [34], the heat release from the heterogeneous oxidation of CO induces an increment of the catalyst temperature, thus favoring methane combustion. This could be an explanation for the CO effect.

Table 2
T_{30} and T_{50} values for the granulated catalyst $La_{0.91}Mn_{0.85}Ce_{0.24}Pd_{0.1}O_z$ after thermal treatment at 750 or 950 °C for several hours (°C)

Catalyst no.	Thermal treatment	0.4% CO		0.0% CO	
		T_{30}	T_{50}	T_{30}	T_{50}
1	–	490	557	495	559
2	750 °C, 3 h, 0.4% CO	495	553	515	574
3	950 °C, 5 h, 0.0% CO	–	–	480	743
4	950 °C, 3 h, 0.4% CO	409	465	434	489
5	950 °C, 5 h, 0.4% CO	399	476	422	488

Table 2 summarizes the methane T_{30} and T_{50} values, corresponding to 30% and 50% conversion of methane, respectively. The samples were either fresh or thermally treated at 750 °C or 950 °C for several hours. All samples were prepared using glycine as complexing agent and applying drying of the precursor solution at 115 °C for 24 h before calcination at 750 °C for 1 h. Table 2 shows that the samples treated at 950 °C for 3 h were the most active, while thermal treatment in the absence of CO, resulted in less active catalysts. The most interesting observation is that a thermally treated catalyst (no. 4) not only exhibits catalytic activity higher than the fresh (no. 1), but also maintains its activity after further exposure at high temperatures (no. 5).

The Pd content in the active phase was studied by keeping a standard Pd loading in the reactor (0.111, 0.222 or 0.444 mmol of Pd) and varying x in $La_{0.91}Mn_{0.85}Ce_{0.24}Pd_xO_z$. To this end, different amounts of $La_{0.91}Mn_{0.85}Ce_{0.24}Pd_xO_z$ were used in each experiment. All samples were prepared using glycine as complexing agent and applying drying of the precursor solution at 115 °C for 24 h before calcination at 750 °C for 1 h. The samples were tested after thermal treatment at 950 °C for 3 h. The T_{50} values are plotted in Fig. 2 as a function of x and of the Pd load. It was not possible to obtain measurements for all combinations of x values and Pd loads because of the limits in minimum and maximum total flowrate that could be applied. The catalytic activity increases with decreasing the Pd content. This can be ascribed to the increase of Pd dispersion in agreement with previous reports [17,35]. The most promising catalyst was that with $x = 0.05$, which corresponds to 2.44 mol% of Pd in the total active phase metals or to 0.185 mmol Pd/g of active phase. Although the catalyst with $x = 0.025$ was more effective, its use instead of the catalyst with $x = 0.05$, would necessitate the deposition of a twofold active phase quantity. Thus, a twofold catalytic layer thickness inside the monolith channels would be induced. Consequently, this could cause high values of pressure drop through the monolith.

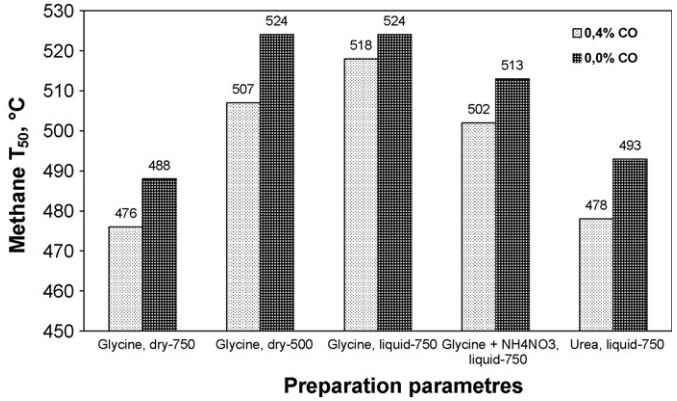

Fig. 1. Methane light off temperatures of the differently prepared $La_{0.91}Mn_{0.85}Ce_{0.24}Pd_xO_z$ ($x = 0.1$) granulated catalysts.

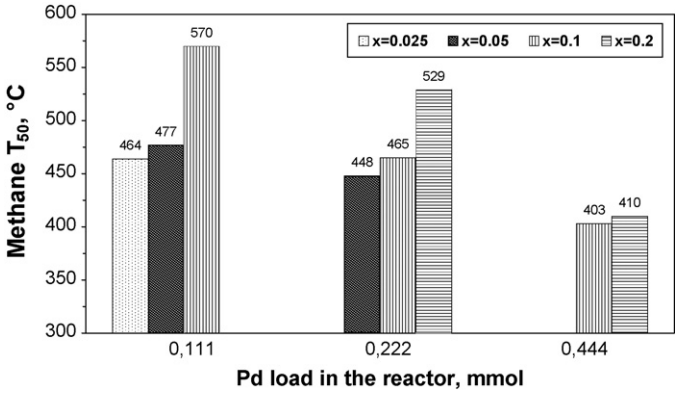

Fig. 2. Methane T_{50} values of the granulated $La_{0.91}Mn_{0.85}Ce_{0.24}Pd_xO_z$ catalyst with different Pd contents in the active phase and different Pd loads in the reactor.

Table 3
Methane T_{30} and T_{50} (°C) data of granulated catalysts, thermally treated at 950 °C for 3 h

Catalyst	0 ppm SO_2		5 ppm SO_2	
	T_{30}	T_{50}	T_{30}	T_{50}
$La_{0.91}Mn_{0.85}Ce_{0.24}Pd_{0.05}O_z$	407	483	415	498
$La_{1.034}Mn_{0.966}Pd_{0.05}O_z$	422	479	428	482
$La_{0.91}Mn_{0.85}Zr_{0.24}Pd_{0.05}O_z$	564	>800	–	–
$La_{0.91}Mn_{0.85}Mg_{0.24}Pd_{0.05}O_z$	>800	>800	–	–
$La_{0.966}Mn_{1.034}Pd_{0.05}O_z$	>800	>800	–	–

Taking into account the already presented experimental results, several modifications of the starting active phase, $La_{0.91}Mn_{0.85}Ce_{0.24}Pd_xO_z$, were examined. The most promising active phases were exposed for 2 h to reactant mixture containing 5 ppm SO_2 for the evaluation of their resistance to sulfur. The methane T_{30} and T_{50} are presented in Table 3. It can be seen that $La_{0.91}Mn_{0.85}Ce_{0.24}Pd_{0.05}O_z$ and $La_{1.034}Mn_{0.966}Pd_{0.05}O_z$ exhibit both, high catalytic activity and adequate resistance to sulfur. Upon reversing the La and Mn contents in $La_{1.034}Mn_{0.966}Pd_{0.05}O_z$, a completely inactive catalyst, $La_{0.966}Mn_{1.034}Pd_{0.05}O_z$, was produced. Also, Ce replacement by Zr led to a less active catalyst, while Ce replacement by Mg resulted in a totally inactive catalyst.

3.1.2. Monolithic catalysts

All the powders that were deposited on cordierite monoliths were prepared using glycine as complexing agent and by applying drying of the precursor solution at 115 °C for 24 h before calcination at 750 °C for 1 h.

The $La_{0.91}Mn_{0.85}Ce_{0.24}Pd_{0.05}O_z$ phase was used for the determination of the active phase load on the monolith, expressed as g Pd ft^{-3} (1 g Pd ft^{-3} = 0.035315 kg Pd m^{-3}). Five monoliths were prepared with Pd loads between 70 and 228 g Pd ft^{-3}. The monoliths were thermally treated at 950 °C for 3 h. The space velocity was kept at 100 000 h^{-1}. The T_{30} and T_{50} values are plotted in Fig. 3. It can be seen that there is essentially no effect for Pd loads higher than 120 g Pd ft^{-3}. Taking into account the results plotted in Fig. 2, it can be concluded that an increase of Pd load on the monolith basis favors catalytic effectiveness only when the Pd content in the active phase is simultaneously decreased ($x < 0.05$). This, however, would cause an increase of the coating thickness, resulting in high pressure drop through the monolith.

In order to study the effect of Pd content (x in Pd_x) on monolithic catalysts, two samples with different Pd content in the active phase, but with, almost, the same Pd loading on the monolith basis were prepared. The first was $La_{1.034}Mn_{0.966}Pd_{0.05}O_z$ with a Pd load of 123.85 g Pd ft^{-3} and the second was $La_{1.034}Mn_{0.966}Pd_{0.09}O_z$ with a Pd load of 123.62 g Pd ft^{-3}. Composition 2 (Table 1) was used for the activity tests. The catalysts were thermally treated at 950 °C for 3 h under composition 3. The space velocity was kept at 50 000 h^{-1}. For both catalysts, at all R_x with or without SO_2 present, the CO conversion was 100% in the whole temperature range (300–800 °C). As seen in Fig. 4a, in a SO_2-free environment, the low Pd content catalyst appeared more active for methane oxidation at R_x = 1.2 and 1.02. It seems that oxidizing conditions favored the low Pd content catalyst. A gradual deactivation of both catalysts was observed at R_x = 0.99 and 0.96 (Fig. 4b). The introduction of 8 ppm SO_2 for 7.5 h in the reactant mixture at R_x = 0.99 (Fig. 5a) caused a significant decrease in methane conversion on the catalyst with x = 0.09 at temperatures between 600 and 710 °C. On the contrary, the low Pd content (x = 0.05) catalyst appeared activated at temperatures 380–570 and 600–650 °C and superior to the catalyst with x = 0.09 at all temperatures. With respect to the NO conversion, Fig. 5b shows that, in the absence of SO_2, the high Pd content catalyst was slightly more effective at 615–670 °C. Insertion of 8 ppm SO_2 affected both catalysts. For x = 0.05, a slight activation and deactivation occurred between 630 and 655 and between 655 and 800 °C, respectively. The SO_2 effect was more profound on the x = 0.09 catalyst, especially in the range 620–730 °C. Figs. 4 and 5a show that, at temperatures higher than 650 °C and for R_x values between 0.96 and 1.02, i.e. representative exhaust conditions, the conversion of methane on $La_{1.034}Mn_{0.966}Pd_{0.05}O_z$ exceeds 85%. This is important because, given its proven thermal stability, such a catalyst could be used in a close-coupled operation mode.

It is interesting that the curves in Figs. 4a and b and 5a, are not of the typical S-type form. Previous experiments in our laboratory

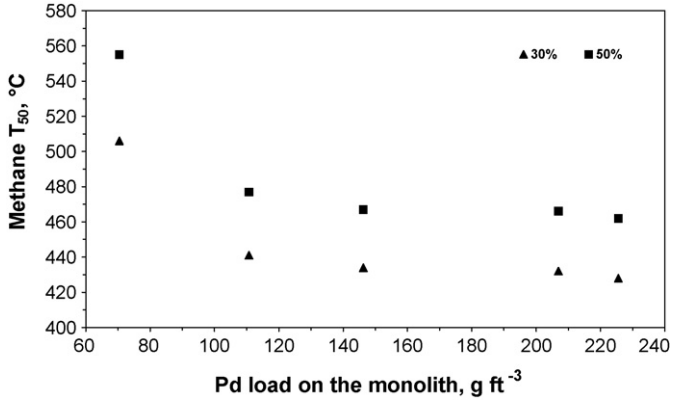

Fig. 3. Dependence of T_{30} and T_{50} of the $La_{0.91}Mn_{0.85}Ce_{0.24}Pd_{0.05}O_z$ monolithic catalyst on Pd load.

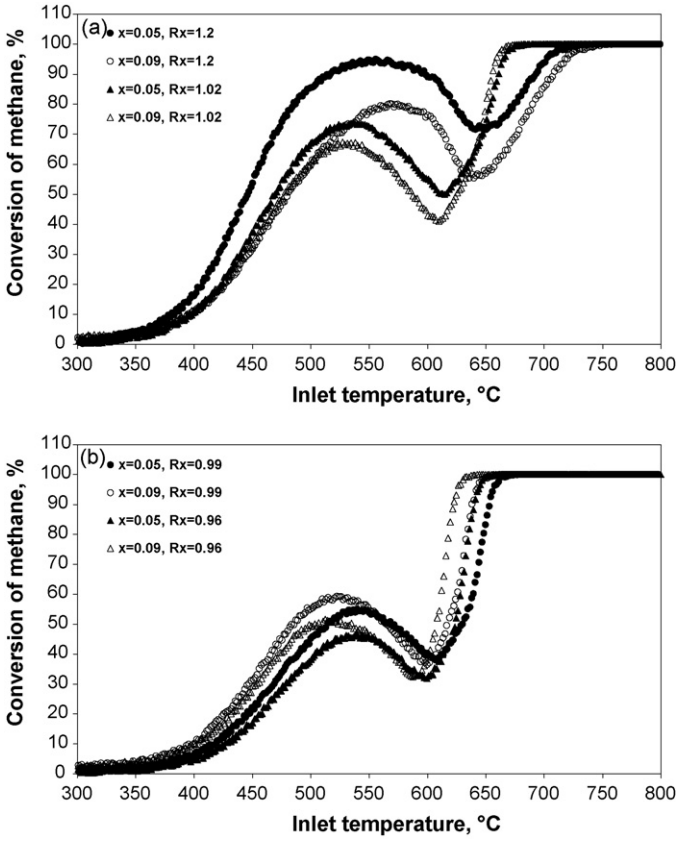

Fig. 4. Temperature dependence of methane conversion of the $La_{1.034}Mn_{0.966}Pd_xO_z$ monolithic catalyst under (a) oxidizing or (b) reducing conditions. Filled symbols: x = 0.05; open symbols: x = 0.09.

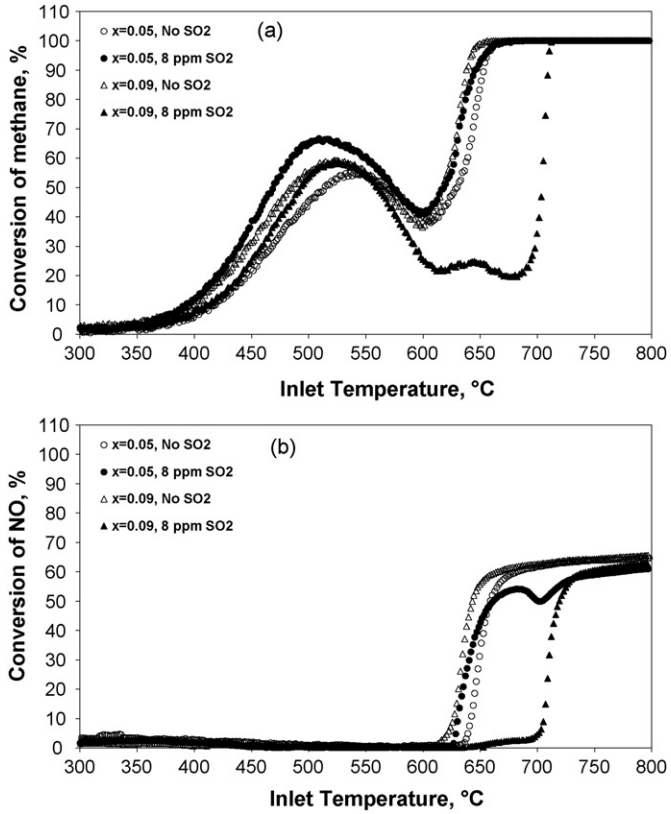

Fig. 5. Effect of SO_2 on the conversion of (a) methane and (b) NO of the $La_{1.034}Mn_{0.966}Pd_xO_z$ monolithic catalyst at $R_x = 0.99$. (●) $x = 0.05$; (▲) $x = 0.09$; open symbols: no SO_2; filled symbols: 8 ppm SO_2.

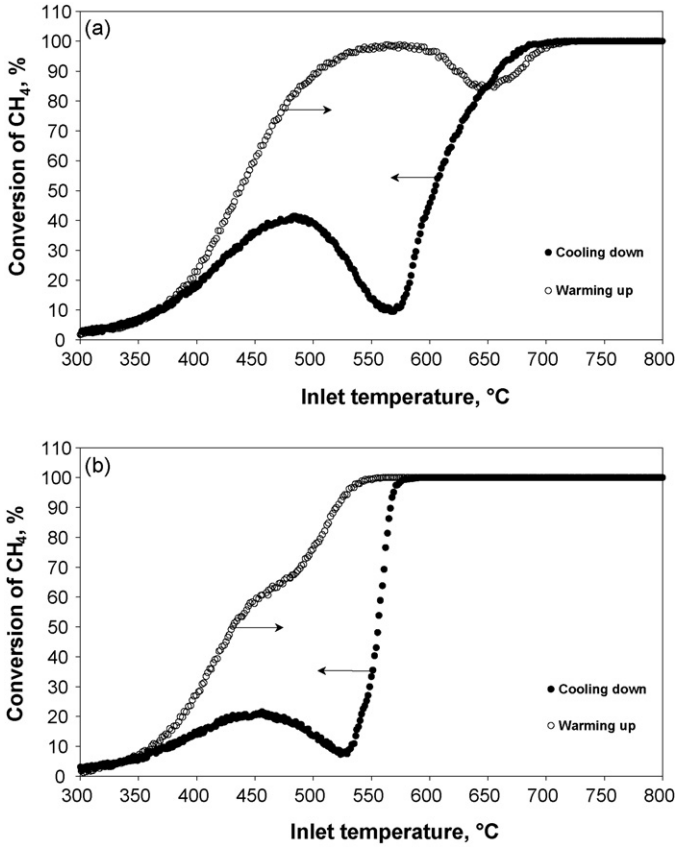

Fig. 6. Dependence of methane conversion on temperature, during temperature fall (left arrows) and rise (right arrows), for the $La_{1.034}Mn_{0.966}Pd_{0.05}O_z$ monolithic catalyst at (a) $R_x = 1.2$ and (b) $R_x = 0.99$.

showed that catalytic performance of Pd containing perovskites depends strongly on the oxidation state of Pd. The Pd oxidation state transitions were investigated using the monolithic catalyst $La_{1.034}Mn_{0.966}Pd_{0.05}O_z$ with a Pd load of 196.25 g Pd ft^{-3}. Compositions 2 and 3 were used for the activity tests and for the thermal treatments at 950 °C for 3 h, respectively. Measurements during cooling down were followed by measurements during warming up, with a space velocity of 50 000 h^{-1}. Fig. 6a and b, show the dependence of methane conversion on temperature at $R_x = 1.2$ and $R_x = 0.99$ respectively. A hysteresis loop was observed between the curves of cooling down and warming up at 390–650 °C for $R_x = 1.2$ and at 360–580 °C for $R_x = 0.99$, respectively. A continuous activation was observed during cooling down from 565 to 480 °C for $R_x = 1.2$ and from 525 to 450 °C for $R_x = 0.99$, while the opposite was observed in the same temperature ranges during warming up. Further deactivation was observed for $R_x = 1.2$ during warming up from 590 to 645 °C. It is suggested that these phenomena are associated to Pd oxidation state transitions. Since lower temperatures favor the formation of PdO, the activation during cooling down may occur because of a transition from the metallic (or close to the metallic) to the Pd^{2+} state. Similarly, the deactivation during warming up can be explained by the temperature rise, which favors PdO decomposition. For $R_x = 0.99$, the state transition occurred at temperatures 30–40 °C lower than for $R_x = 1.2$, because a lower oxygen partial pressure pushes the equilibrium of the reaction $PdO \leftrightarrow Pd^0 + (1/2)O_2$ to the right.

Table 4
BET SSAs of various catalytic powders

	Catalyst	Preparation	Thermal treatment		SSA ($m^2\ g^{-1}$)
			T (°C), time (h)	Environment	
1	$La_{0.91}Mn_{0.85}Ce_{0.24}Pd_{0.1}O_z$	Dry-750	Fresh	–	36.8
2	$La_{0.91}Mn_{0.85}Ce_{0.24}Pd_{0.1}O_z$	Dry-750	950 °C, 3 h	RM[a] 0.0% CO	9.8
3	$La_{0.91}Mn_{0.85}Ce_{0.24}Pd_{0.1}O_z$	Dry-750	950 °C, 3 h	RM 0.4% CO	16.6
4	$La_{0.91}Mn_{0.85}Ce_{0.24}Pd_{0.1}O_z$	Liquid-500 NH_4NO_3	Fresh	–	15.1
5	$La_{0.91}Mn_{0.85}Zr_{0.24}Pd_{0.05}O_z$	Dry-750	Fresh	–	45.5
6	$La_{0.91}Mn_{0.85}Zr_{0.24}Pd_{0.05}O_z$	Dry-750	950 °C, 3 h	RM 0.4% CO	9.5
7	$La_{0.91}Mn_{0.85}Mg_{0.24}Pd_{0.05}O_z$	Dry-750	Fresh	–	40.6
8	$La_{0.91}Mn_{0.85}Mg_{0.24}Pd_{0.05}O_z$	Dry-750	950 °C, 3 h	RM 0.4% CO	10.6
9	$La_{1.034}Mn_{0.966}Pd_{0.05}O_z$	Dry-750	Fresh	–	25.8
10	$La_{1.034}Mn_{0.966}Pd_{0.05}O_z$	Dry-750	950 °C, 3 h	RM 0.4% CO	13.6

[a] Reactant mixture.

3.2. Characterization

3.2.1. BET

The BET SSA measurements are shown in Table 4. Incorporation, in fresh catalysts, of Ce, Zr and Mg incurred an increase in SSA in the order Zr (5) > Mg (7) > Ce (1). After thermal treatment at 950 °C for 3 h, only the Ce (3) containing catalyst retained a relatively high SSA and the order changed to Ce (3) > Mg (8) > Zr (6). This observation is in good agreement with previous works reporting that lanthanum manganites, partially substituted by Ce retained high SSA after high-temperature thermal treatment [36]. The catalyst prepared using NH_4NO_3, (4), exhibited the lowest fresh state SSA, probably because of the high-temperature rise in the bulk of the prepared powder during calcination. A comparison of (2) and (3) indicates that CO presence favors higher SSA. Although the SSAs measured are low compared to common catalytic materials, their values are in the range 10–45 $m^2\,g^{-1}$, i.e. comparable to the SSAs of other perovskites. Another interesting observation is that samples with lower SSA are more active, e.g. (1) vs. (3) in Table 4 which correspond to (1) vs. (4) in Table 2.

3.2.2. XRD

The XRD spectra of various $La_{0.91}Mn_{0.85}Ce_{0.24}Pd_{0.1}O_z$ samples are shown in Fig. 7. Pattern (1) implies that an amorphous material was obtained at 500 °C. Pattern (2) shows that after thermal treatment at 950 °C for 3 h, the $LaMnO_3$ perovskite phase was well crystallized. Patterns (3) and (4) show that crystallization was achieved at 750 °C, while pattern (5) indicates an "extension" of crystallization at 950 °C. Crystalline CeO_2 was detected in all the high-temperature treated samples. Although it has been reported [36] that Ce can be a substitute in $LaMnO_3$, it is possible that Ce could not enter the perovskite structure. The small peak that appears next to the main perovskite peak, can be ascribed to PdO or $La_2Pd_2O_5$. This peak appeared strong in the high-temperature treated and was almost absent in the fresh samples. Thus, it is suggested that in the fresh samples, Pd was fully, or to a large extent, inserted in the perovskite structure, resulting in a moderate catalytic activity. After thermal treatment at 950 °C, it appeared as a separate phase, PdO, causing a significant activation in methane combustion, as seen in Table 2. Similar structural and activity characteristics were observed by Zhou et al. [20] on the Pd/$LaFe_{0.8}Co_{0.2}O_3$ and the $LaFe_{0.77}Co_{0.17}Pd_{0.06}O_3$ perovskite systems for the gasoline TWC application. Pattern (6) shows that the use of NH_4NO_3 allowed better crystallization at 750 °C. Insignificant changes of the perovskite crystallization occurred after thermal treatment of this sample at 950 °C for 3 h, pattern (7), indicating that, when NH_4NO_3 is introduced in the precursor solution, a high-temperature rise occurs in the bulk of the powders.

The XRD patterns of fresh dry-750 and thermally treated for 3 h at 950 °C, are shown in Fig. 8a and b, respectively. Patterns (5) and (6), show that in the fresh catalysts, the structures containing La, Mn and Pd only, were better crystallized. The $LaMnO_3$ perovskite formation at lower calcination temperatures, 650 or 700 °C, has been reported in the literature [29,36,37]. Crystallization of ceria appeared at inchoative stage. This is also in agreement with previous works reporting the lower crystallization degree of $La_{1-x}Ce_xMnO_3$ treated at 700 °C, and the formation of segregated CeO_2 after thermal treatment at 800 °C [36]. In contrast to ceria, no Mg or Zr oxides were detected, indicating that they were either amorphous, or incorporated to the perovskite structure. The PdO peak was well configured in the high Pd content ($Pd_{0.2}$) sample but it was hardly discernible in the low Pd content ($Pd_{0.05}$) catalysts. A better crystallization of the perovskite was achieved after thermal treatment at 950 °C for 3 h, as seen in Fig. 8b. CeO_2 appeared as a separate phase in agreement to literature reports, while Mg and Zr were probably inserted into the perovskite structure [38]. The PdO peak was detected only in the high Pd pattern. It is very interesting that another peak appeared in the patterns of non-Ce containing catalysts at 37.7°. This peak was similar, but not fitting exactly, to those of $La_2Pd_2O_8$ or PdO_2 and, most probably, corresponds to an oxidized Pd^{x+} form, with $x > 2$.

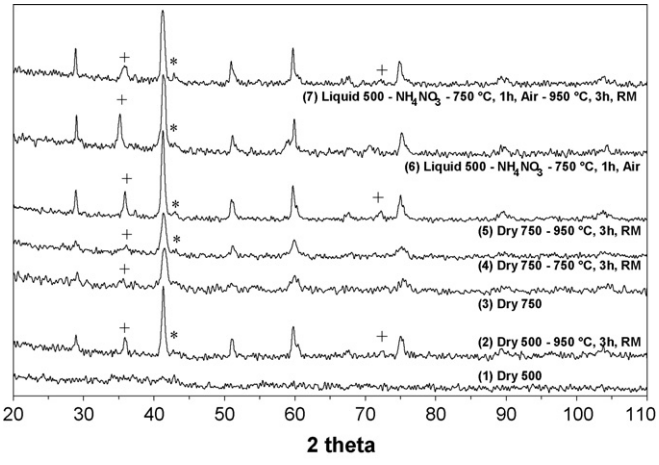

Fig. 7. XRD patterns of fresh dry-750 and thermally treated $La_{0.91}Mn_{0.85}Ce_{0.24}Pd_xO_z$ ($x = 0.1$) samples. RM: reaction mixture; +: CeO_2; *: PdO. The non-characterized by symbol peaks correspond to the $LaMnO_3$ perovskite.

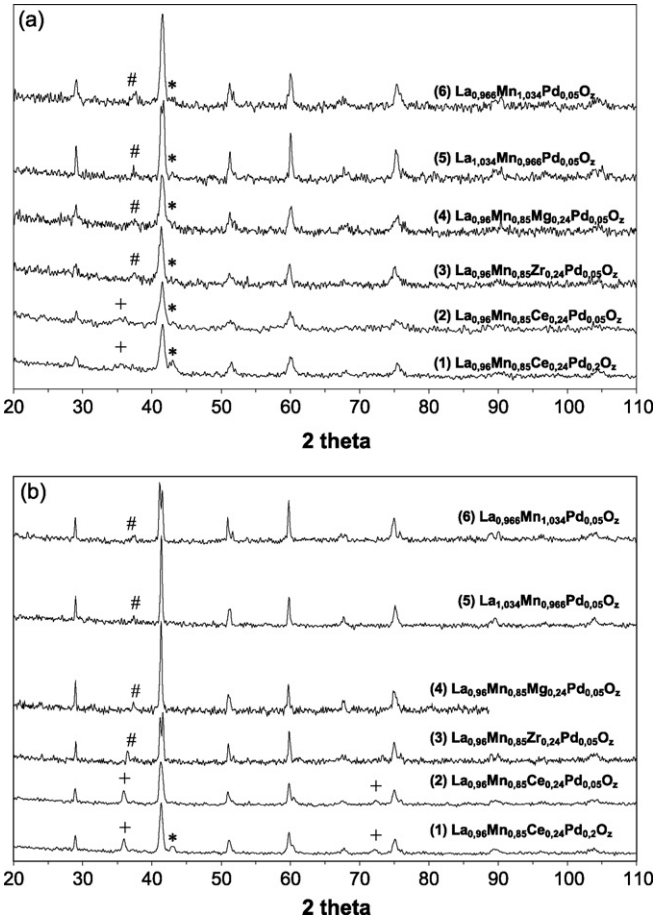

Fig. 8. XRD patterns of (a) fresh dry-750 and (b) thermally treated at 950 °C for 3 h. +: CeO_2; *: PdO; #: PdO_2 or $La_2Pd_2O_8$. The peaks with no symbol correspond to the $LaMnO_3$ perovskite.

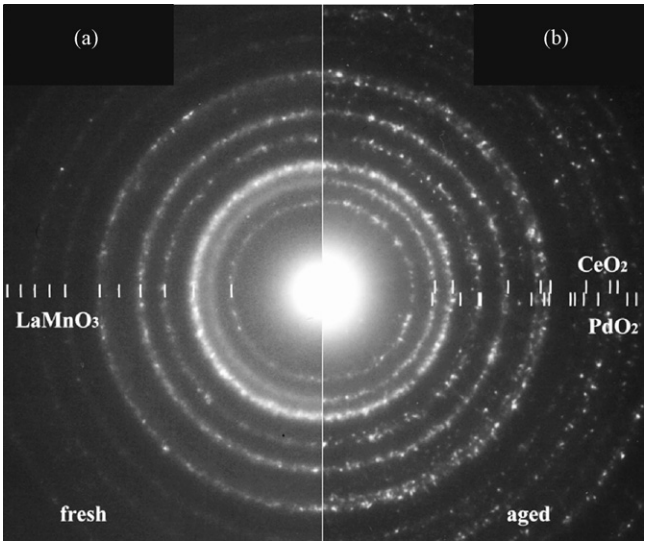

Fig. 9. Electron diffraction images of (a) fresh dry-750 and (b) thermally treated, 1000 °C for 10 h in air, of the $La_{0.91}Mn_{0.85}Ce_{0.24}Pd_{0.1}O_z$ catalyst.

3.2.3. TEM

TEM analysis was carried out on fresh dry-750 and thermally treated (for 10 h at 1000 °C in air) $La_{0.91}Mn_{0.85}Ce_{0.24}Pd_{0.1}O_z$ catalysts. Fig. 9a and b shows the electron diffraction images of the fresh and treated samples. It can be seen that both materials were polycrystalline and no obvious phase transition occurred after thermal treatment. The cubic $LaMnO_3$ perovskite was found as the main phase of the catalytic material, while the more distinguishable spots appeared at the aged sample, indicated an increase of the average crystallite size.

Micrographs of fresh and treated samples are shown in Fig. 10a and b, respectively. The small crystallite that appeared in Fig. 10a, having a size of 4.2 nm and a distance of lattice planes (d) of 0.315 nm, can be ascribed to cubic CeO_2 ($d_{1\,1\,1}$ = 0.312 nm) or to tetragonal PdO_2 ($d_{1\,1\,0}$ = 0.318 nm). The coexistence of both phases cannot be excluded, since the formation of PdO_2 was of high probability according to the XRD results. The crystallites with sizes 13.9 and 16.8, and 0.394 nm distance between lattice planes, correspond to the cubic $LaMnO_3$ phase ($d_{1\,0\,0}$ = 0.388 nm). From Fig. 10b, it is concluded that thermal treatment caused an increase in crystallite size. The size of the crystallite shown was ~30 nm. No PdO and metallic Pd were detected in either sample, indicating again the Pd insertion in the perovskite structure.

3.2.4. XPS

Table 5 contains XPS analysis of fresh dry-750 and thermally treated (at 950 °C for 3 h) catalysts. The La surface composition appears lower than that of the bulk, while the opposite is observed for Mn. In all samples, the surface Pd content was lower than that in the bulk. From the last two columns of Table 5, the ratio of surface to bulk Pd can be calculated. It was found that this ratio increases with decreasing x. This verifies the T_{50} results presented in Fig. 2.

The La 3d and Ce 3d binding energies (BE) varied considerably. The BEs in the range 834.2 ± 0.4 eV for La 3d and 881.9 ± 0.3 eV for Ce 3d have been ascribed to La^{3+} and Ce^{4+} [39]. An XPS peak fitting software (XPSPeak Version 4.1) was used for the analysis of the Mn 2p and Pd 3d peaks. As seen in Fig. 11a, the Mn total peak (raw data) in thermally treated $La_{0.91}Mn_{0.85}Ce_{0.24}Pd_{0.1}O_z$, can be analyzed into two peaks. Peak fitting of the rest of the samples resulted in about the same BEs. The peak at 641.8 eV corresponded to Mn^{2+} and Mn^{3+} [39],

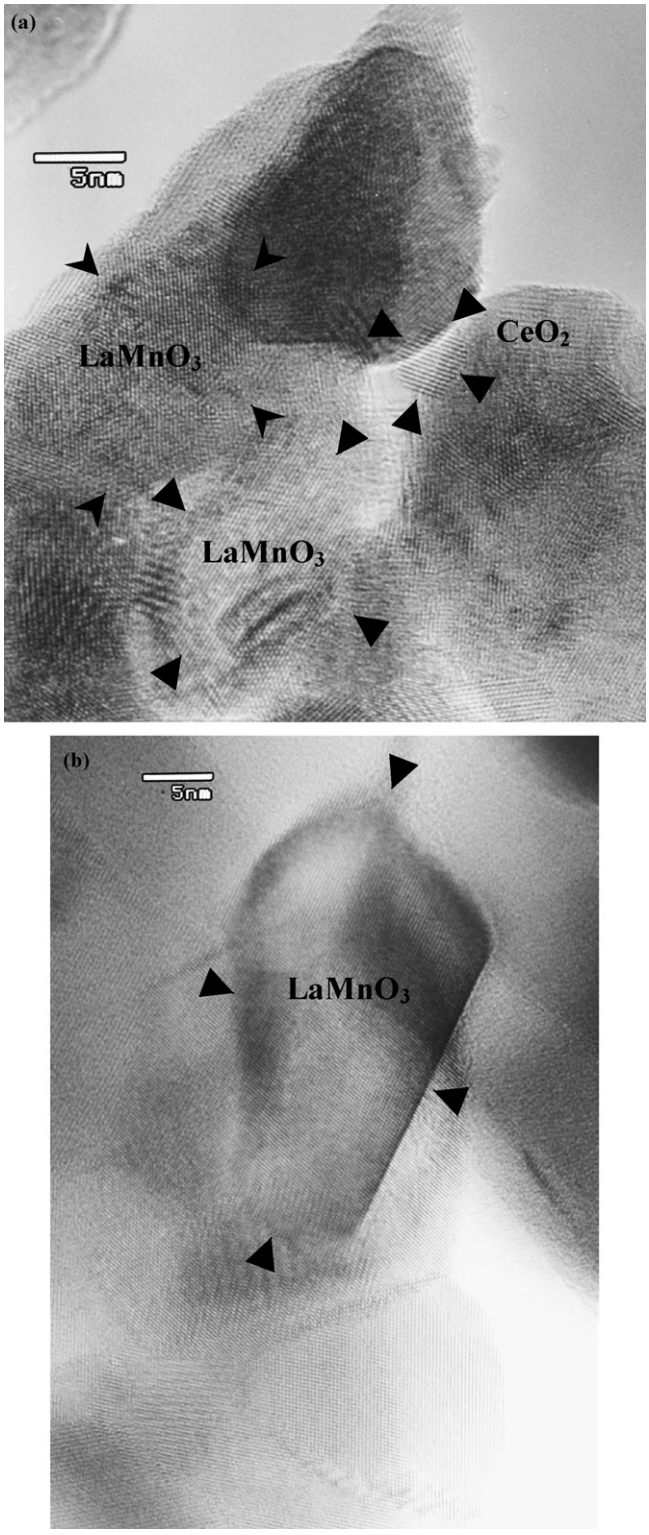

Fig. 10. High resolution electron micrographs of (a) fresh dry-750 and (b) thermally treated at 1000 °C for 10 h in air, of the $La_{0.91}Mn_{0.85}Ce_{0.24}Pd_{0.1}O_z$ catalyst.

while the less intense peak at 644.6 eV, is probably due to Mn^{x+}, $x > 3$. The BEs of La 3d and Mn 2p of the examined samples were too close to the BEs of $LaMnO_3$, providing strong evidence that the perovskite structure was formed on the catalytic surface and that La and Mn were not segregated as simple oxides. The La 3d and Mn 2p BEs are in good agreement with those reported by Sinquin et al. [40], who attributed the peak at 833.7 eV, to La^{3+} of $LaMnO_3$.

Table 5
XPS surface and nominal bulk composition of fresh and thermally treated catalysts

Catalyst	La (mol%)		Mn (mol%)		Ce (mol%)		Pd (mol%)	
	Surface	Bulk	Surface	Bulk	Surface	Bulk	Surface	Bulk
Fresh catalysts dry-750								
$La_{0.91}Mn_{0.85}Ce_{0.24}Pd_{0.05}O_z$	38.4	44.4	44.3	41.5	15.4	11.7	1.9	2.4
$La_{0.91}Mn_{0.85}Ce_{0.24}Pd_{0.1}O_z$	36.7	43.3	40.8	40.5	20.2	11.4	2.2	4.8
$La_{1.034}Mn_{0.966}Pd_{0.05}O_z$	46.0	50.4	52.1	47.1	–	–	1.9	2.4
$La_{0.966}Mn_{1.034}Pd_{0.05}O_z$	43.1	47.1	55.7	50.4	–	–	1.2	2.4
Thermally treated, 950 °C for 3 h under reactant mixture								
$La_{0.91}Mn_{0.85}Ce_{0.24}Pd_{0.025}O_z$	38.6	44.9	39.3	42.0	21.2	11.9	0.9	1.2
$La_{0.91}Mn_{0.85}Ce_{0.24}Pd_{0.05}O_z$	39.0	44.4	42.3	41.5	17.1	11.7	1.7	2.4
$La_{0.91}Mn_{0.85}Ce_{0.24}Pd_{0.1}O_z$	37.5	43.3	41.8	40.5	18.5	11.4	2.3	4.8
$La_{0.91}Mn_{0.85}Ce_{0.24}Pd_{0.2}O_z$	36.9	41.4	41.2	38.6	17.5	10.9	4.4	9.1
$La_{1.034}Mn_{0.966}Pd_{0.05}O_z$	49.0	50.4	49.6	47.1	–	–	1.4	2.4
$La_{0.966}Mn_{1.034}Pd_{0.05}O_z$	43.1	47.1	54.6	50.4	–	–	2.3	2.4

Table 6
BEs and proportion of Pd 3d peaks

Catalyst	BE (eV)		% Peak 1–% Peak 2
	Peak 1 (Pd^{2+})	Peak 2 (Pd^{x+}, $x > 2$)	
Fresh catalysts, dry-750			
$La_{0.91}Mn_{0.85}Ce_{0.24}Pd_{0.05}O_z$	337.3	–	100.0–0.0
$La_{0.91}Mn_{0.85}Ce_{0.24}Pd_{0.1}O_z$	337.2	–	100.0–0.0
$La_{1.034}Mn_{0.966}Pd_{0.05}O_z$	336.9	339.2	83.3–16.7
$La_{0.966}Mn_{1.034}Pd_{0.05}O_z$	336.9	339.1	90.9–9.1
Aged catalysts, 950 °C for 3 h under reactant mixture			
$La_{0.91}Mn_{0.85}Ce_{0.24}Pd_{0.025}O_z$	337.1	–	100.0–0.0
$La_{0.91}Mn_{0.85}Ce_{0.24}Pd_{0.05}O_z$	336.9	338.9	76.9–23.1
$La_{0.91}Mn_{0.85}Ce_{0.24}Pd_{0.1}O_z$	337.0	339.2	73.5–26.5
$La_{0.91}Mn_{0.85}Ce_{0.24}Pd_{0.2}O_z$	336.9	339.1	84.7–15.3
$La_{1.034}Mn_{0.966}Pd_{0.05}O_z$	336.9	339.2	83.3–16.7
$La_{0.966}Mn_{1.034}Pd_{0.05}O_z$	337.1	335.3[a]	66.7–33.3[a]

[a] Corresponds to metallic Pd.

The Pd 3d peak analysis of thermally treated $La_{0.91}Mn_{0.85}Ce_{0.24}Pd_{0.2}O_z$, showed that the peak consisted of two peaks (Fig. 11b). The first peak appeared at 336.9 eV and corresponds to oxidized Pd^{2+} and the second appeared at 339.1 eV, which corresponds to oxidized Pd^{x+}, $x > 2$ [39]. Similar BEs were reported [21] and were ascribed to cationic Pd^{3+} or Pd^{4+}, inserted at the B-site of $LaFe_{0.95}Pd_{0.05}O_3$ under oxidizing conditions. The high-valence Pd was not observed in all catalysts. Results of the analysis of the Pd 3d peaks are listed in Table 6. It can be seen that for the thermally treated $La_{0.91}Mn_{0.85}Ce_{0.24}Pd_xO_z$, when x in Pd_x decreases from 0.1 to 0.025, the percentage of high-valenced Pd decreases as well. Taking into account that the catalytic activity increases with decreasing the Pd content, it may be concluded that the high-valence Pd is not as active as Pd^{2+}. The enhanced Pd dispersion, however, implies higher catalytic activity. Thus, the above suggestion is not supported strongly. A comparison between $La_{0.91}Mn_{0.85}Ce_{0.24}Pd_{0.05}O_z$ and $La_{1.034}Mn_{0.966}Pd_{0.05}O_z$ shows that the former exhibits better Pd dispersion (the ratios of surface to bulk Pd are 1.7/2.4 and 1.4/2.4, respectively). Nevertheless, as shown in Table 3, the T_{50}, for $La_{1.034}Mn_{0.966}Pd_{0.05}O_z$ is lower and this can be ascribed to its lower percentage of surface high-valenced Pd (16.7% and 23.1%, respectively). The Pd 3d peak at 335.3 eV for $La_{0.966}Mn_{1.034}Pd_{0.05}O_z$ can be ascribed to metallic Pd [39]. This was the only sample in which metallic Pd appeared and was also a totally inactive catalyst. The excess Mn could inhibit either the insertion of Pd in the perovskite lattice or the synergism between Pd and perovskite. In either case, Pd would have been retained unsheltered against reduction.

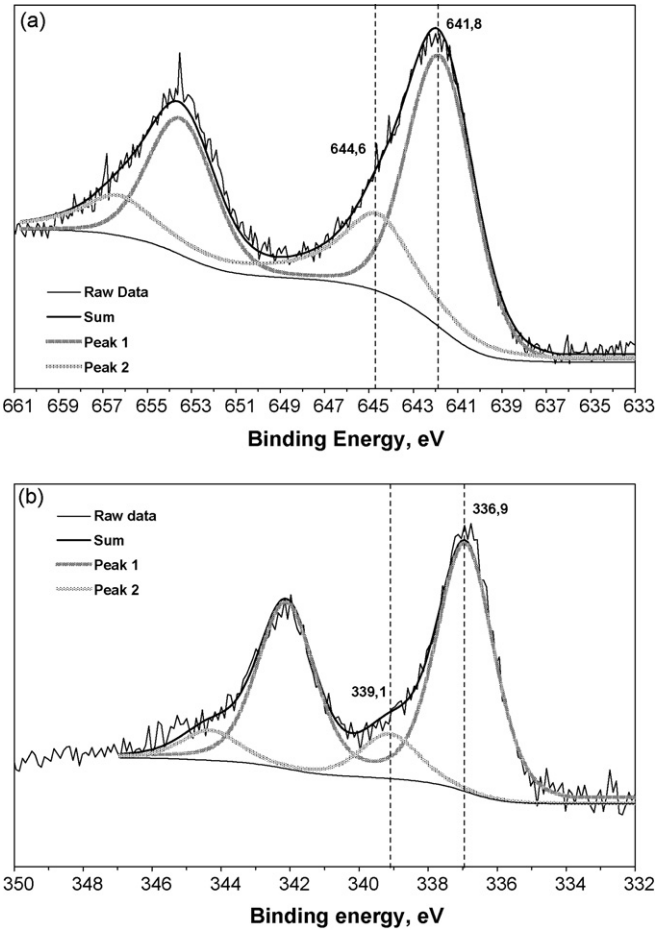

Fig. 11. Peak fitting analysis of (a) Mn 2p in $La_{0.91}Mn_{0.85}Ce_{0.24}Pd_{0.1}O_z$ thermally treated catalyst and (b) Pd 3d in the $La_{0.91}Mn_{0.85}Ce_{0.24}Pd_{0.2}O_z$ thermally treated catalyst.

4. Conclusions

Slight modifications on the preparation procedure of Pd-containing perovskites can cause considerable changes in catalytic activity. The most active catalysts are obtained by a combined sol–gel and combustion synthesis method using glycine as complexing agent and applying drying at 115 °C for 24 h followed by calcination at 750 °C. Thermal treatment at 950 °C for 3 h under reactant mixture, leads to activation which remains unaffected

after further thermal treatment at 950 °C for 2 h, establishing the high thermal stability of the catalysts. The activation by thermal treatment can be ascribed to the migration of Pd from the perovskite lattice of fresh catalysts to segregated PdO.

XPS analysis and catalytic activity tests showed that, under oxidizing conditions, a low Pd content in the active phase favors catalytic activity due to better dispersion of oxidized Pd^{x+}, $2 \leq x \leq 4$, on the catalytic surface. The less oxidized Pd^{2+} appears more active than Pd^{x+}, $x > 2$. Excess Mn in La–Mn–Pd incurs the formation of metallic Pd, resulting in a completely inactive catalyst. On the contrary, Mn deficiency appears to protect Pd against reduction, probably, because Pd occupies Mn vacancies in the perovskite lattice.

The $La_{1.034}Mn_{0.966}Pd_{0.05}O_z$, deposited on cordierite monolith exhibits superior performance under oxidizing or sur-stoichiometric conditions and inferior under sub-stoichiometric conditions compared to $La_{1.034}Mn_{0.966}Pd_{0.09}O_z$. The former appears activated under an 8 ppm SO_2 environment while the latter appears deactivated. Under oxidizing conditions, activation and deactivation during cooling down and warming up, respectively, of $La_{1.034}Mn_{0.966}Pd_{0.05}O_z$ catalyst, can be attributed to Pd oxidation state transitions between the metallic and the oxidized state of Pd.

$La_{0.91}Mn_{0.85}Ce_{0.24}Pd_{0.05}O_z$ and $La_{1.034}Mn_{0.966}Pd_{0.05}O_z$ appear to be promising candidates for TWCs for stoichiometrically operating NGFVs because of their high thermal stability and sulfur resistance. The use of these materials of low noble metal load, 120 g Pd ft^{-3}, implies an almost threefold decrease in cost compared to the currently used Pd/Al_2O_3 catalysts that contain about 300 g noble metals ft^{-3}. Prolonged ageing and sulfur resistance tests are already in progress in order an overall view of the their catalytic behavior to be obtained.

Acknowledgement

The authors gratefully acknowledge the European Union for financial support of this work under contract G5RD-CT2001-00567 (CAT-NAT: Cost-Effective and Durable Nanostructured Pd Catalysts for Natural gas Vehicle and premixed Burner Applications).

References

[1] C.S. Weaver, SAE Tech. Pap. No. 892133, 1989.
[2] R.J. Farrauto, R.M. Heck, Catal. Today 51 (1999) 351.
[3] J.K. Lampert, M. Shahjahan Kazi, R.J. Farrauto, Appl. Catal. B: Environ. 14 (1997) 211.
[4] R.M. Heck, R.J. Farrauto, Appl. Catal. A: Gen. 221 (2001) 443.
[5] F. Klingstedt, A. Kalandar Neyestanaki, R. Byggningsbacka, L.-E. Lindfors, M. Lunden, M. Petersson, P. Tengstrom, T. Ollonqvist, J. Vayrynen, Appl. Catal. A: Gen. 209 (2001) 301.
[6] P. Gelin, M. Primet, Appl. Catal. B: Environ. 39 (2002) 1.
[7] T. Seiyama, in: L.G. Tejuka, J.L.G. Fierro (Eds.), Properties and Applications of Perovskite-Type Oxides, Marcel Dekker, 1993, p. 215.
[8] S. Cimino, L. Lisi, R. Pirone, G. Russo, M. Turco, Catal. Today 59 (2000) 19.
[9] E. Campagnoli, A. Tavares, L. Fabbrini, I. Rossetti, Yu.A. Dubitsky, A. Zaopo, L. Forni, Appl. Catal. B: Environ. 55 (2005) 133.
[10] S. Petrovic, V. Rakic, D.M. Jovanovic, A.T. Baricevic, Appl. Catal. B: Environ. 66 (2006) 249.
[11] U.G. Singh, J. Li, J.W. Bennett, A.M. Rappe, R. Seshadri, S.L. Scott, J. Catal. 249 (2007) 349.
[12] R. Zhang, H. Alamdari, S. Kaliaguine, J. Catal. 242 (2006) 241.
[13] J.-M. Giraudon, A. Elhachimi, F. Wyrwalsky, S. Siffert, A. Aboukais, J.-F. Lamonier, G. Leclercq, Appl. Catal. B: Environ. 75 (2007) 157.
[14] S. Cimino, G. Landi, L. Lisi, G. Russo, Catal. Today 117 (2006) 454.
[15] V.R. Choudhary, B.S. Uphade, S.G. Pataskar, Fuel 78 (1999) 919.
[16] F. Cifa, P. Dinka, P. Viparelli, S. Lancione, G. Benedetti, P.L. Villa, M. Viviani, P. Nanni, Appl. Catal. B: Environ. 46 (2003) 463.
[17] S. Petrovic, L. Karanovic, P.K. Stefanov, M. Zdujic, A. Terlecki-Baricevic, Appl. Catal. B: Environ. 58 (2005) 133.
[18] A. Civera, G. Negro, S. Specchia, G. Saracco, V. Specchia, Catal. Today 100 (2005) 275.
[19] N. Guilhaume, M. Primet, J. Catal. 165 (1997) 197.
[20] K. Zhou, H. Chen, Q. Tian, Z. Hao, D. Shen, X. Xu, J. Mol. Catal. A: Chem. 189 (2002) 225.
[21] M. Uenishi, M. Taniguchi, H. Tanaka, M. Kimura, Y. Nishihata, J. Mizuki, T. Kobayashi, Appl. Catal. B: Environ. 57 (2005) 267.
[22] R. Zhang, H. Alamdari, S. Kaliaguine, Appl. Catal. B: Environ. 72 (2007) 331.
[23] D. Fino, N. Russo, G. Saracco, V. Specchia, Progr. Solid State Chem. 35 (2007) 501.
[24] J. Twu, P.K. Gallagher, in: L.G. Tejuka, J.L.G. Fierro (Eds.), Properties and Applications of Perovskite-Type Oxides, Marcel Dekker, 1993, p. 1.
[25] M.M. Natile, E. Ugel, C. Maccato, A. Glisenti, Appl. Catal. B: Environ. 72 (2007) 351.
[26] A.E. Giannakas, A.K. Ladavos, P.J. Pomonis, Appl. Catal. B: Environ. 49 (2004) 147.
[27] C. Oliva, L. Bonoldi, S. Cappelli, L. Fabbrini, I. Rossetti, L. Forni, J. Mol. Catal. A: Chem. 226 (2005) 33.
[28] P. Gelin, L. Urfels, M. Primet, E. Tena, Catal. Today 83 (2003) 45.
[29] M. Alifanti, R. Auer, J. Kirchnerova, F. Thyrion, P. Grange, B. Delmon, Appl. Catal. B: Environ. 41 (2003) 71.
[30] I. Rosso, E. Garrone, F. Geobaldo, B. Onida, G. Saracco, V. Specchia, Appl. Catal. B: Environ. 30 (2001) 61.
[31] L. Wan, in: L.G. Tejuka, J.L.G. Fierro (Eds.), Properties and Applications of Perovskite-Type Oxides, Marcel Dekker, 1993, p. 145.
[32] F. Klingstedt, H. Karhu, A. Kalantar Neyestenaki, L.-E. Lindfors, T. Salmi, J. Vayrynen, J. Catal. 206 (2002) 248.
[33] T. Maillet, C. Solleau, J. Barbier Jr., D. Duprez, Appl. Catal. B: Environ. 14 (1997) 85.
[34] S. Cimino, A. Di Benedetto, R. Pirone, G. Russo, Catal. Today 83 (2003) 33.
[35] M.J. Koponen, T. Venalainen, M. Suvanto, K. Kallinen, T.-J.J. Kinnunen, M. Harkonen, T.A. Pakanen, J. Mol. Catal. A: Chem. 258 (2006) 246.
[36] M. Alifanti, J. Kirchnerova, B. Delmon, Appl. Catal. A: Gen. 245 (2003) 231.
[37] Y. Liu, H. Zheng, J. Liu, T. Zhang, Chem. Eng. J. 89 (2002) 213.
[38] G. Saracco, F. Geobaldo, G. Baldi, Appl. Catal. B: Environ. 20 (1999) 277.
[39] NIST, X-ray Photoelectron Spectroscopy Standard Reference Database 20, Version 3.2, National Institute of Standards and Technology, USA, 2000.
[40] G. Sinquin, J.P. Hindermann, C. Petit, A. Kiennemann, Catal. Today 54 (1999) 107.